Dynamics of the Equatorial Mesosphere Observed Using the Jicamarca MST Radar during June and August 1987

DAVID C. FRITTS AND LI YUAN

Geophysical Institute, University of Alaska, Fairbanks, Alaska

MATTHEW H. HITCHMAN

Meteorology Department, University of Wisconsin, Madison, Wisconsin

LAWRENCE COY

Department of Earth and Atmospheric Sciences, St. Louis University, St. Louis, Missouri

ERHAN KUDEKI

Department of Electrical and Computer Engineering, University of Illinois, Champaign, Illinois

RONALD F. WOODMAN

Instituto Geofisico del Peru, Radio Observatorio de Jicamarca, Lima, Peru

(Manuscript received 17 April 1991, in final form 7 October 1991)

ABSTRACT

The Jicamarca MST radar was used in two campaigns during June and August 1987 to measure wave influences, flow variability, and mean structure in the equatorial stratosphere and mesosphere. This paper presents observations of motions and momentum fluxes in the mesosphere during each campaign. A companion paper by Hitchman et al. addresses the mean structure and fluxes as well as comparisons with other datasets. Results presented here indicate that the equatorial mesosphere is dynamically very active, with considerable gravity-wave and tidal motions and persuasive evidence of inertial instability and wave-filtering processes. Vertical velocities at high frequencies are comparable to those observed at other locations. Hourly mean horizontal motions and momentum fluxes are likewise large and variable, exhibiting enormous vertical shears and strong modulation of the wave spectrum and momentum fluxes at higher frequencies. Daily mean profiles reveal persistent structures with vertical scales of ~6–10 km, vertical shears of the meridional velocity of ~0.03 s^{-1}, and large mean momentum fluxes. Also discussed are the implications of these observations for wave forcing and instability in the equatorial middle atmosphere.

1. Introduction

The dynamics of the equatorial middle atmosphere has received increasing attention in the two decades following the discovery of the quasi-biennial oscillation (QBO) in the lower stratosphere and the semiannual oscillation near the stratopause (SSAO) and mesopause (MSAO). As a result, the major characteristics of these oscillations are now reasonably well defined. Much of our knowledge of the QBO, SSAO, and MSAO and the equatorial wave motions that contribute to their forcing has resulted from rawinsonde and rocketsonde wind and temperature measurements (Reed 1965, 1966; Yanai and Maruyama 1966; Wallace and Kousky 1968; Angell and Korshover 1970; Wallace 1973; Nastrom and Belmont 1975; Belmont et al. 1975; Hopkins 1975; Hirota 1978, 1980; Hamilton 1982; Devarajan et al. 1985; Naujokat 1986). Additional information has come from satellite-derived wind and temperature fields (Salby et al. 1984; Dunkerton and Delisi 1985a,b; Hitchman and Leovy 1986, 1988; Hitchman et al. 1987; Gao et al. 1987; Delisi and Dunkerton 1988a,b). Finally, recent theoretical and modeling studies have examined a number of wave and instability processes that provide insights into QBO, SSAO, and MSAO forcing, the structure of the equatorial middle atmosphere, and coupling to higher-latitude phenomena (Dunkerton 1981, 1982, 1983, 1985; Boyd 1982; Boyd and Christidis 1982; Takahashi 1984; Hamilton and Mahlman 1988). Despite these efforts, however, major uncertainties remain concern-

Corresponding author address: Dr. David C. Fritts, LASP, Campus Box 392, University of Colorado, Boulder, CO 80309-0392.

ing the role of various wave motions in the forcing of equatorial oscillations.

The QBO, SSAO, and MSAO, and their associated meridional circulations and thermal and constituent distributions, are now believed to be driven in their eastward and westward phases by a combination of equatorially trapped Kelvin and mixed Rossby–gravity waves, internal gravity waves, and extratropical planetary Rossby waves. Studies by Holton and Lindzen (1972), Plumb (1977), Plumb and McEwan (1978), Plumb and Bell (1982), and Dunkerton (1982, 1985) have suggested the viability of these motions, in various combinations, in providing flow accelerations and evolution of the mean fields qualitatively like those observed. Yet it remains unclear quantitatively which motions provide the primary forcing at different levels. For example, Dunkerton (1985) concluded that the theory by Holton and Lindzen (1972) describes properly the QBO forcing near the equator, but appears not to provide sufficient body forces in either acceleration phase away from the equator.

The modeling effort by Hamilton and Mahlman (1988) and the observational study by Hitchman and Leovy (1988) likewise suggested that westward SSAO accelerations may be driven largely by the residual circulation in the summer hemisphere and planetary wave Eliassen–Palm fluxes in the winter hemisphere, rather than by mixed Rossby–gravity waves, and that Kelvin waves likely play a smaller role in the eastward SSAO phase than suggested by Dunkerton (1981). There is general agreement that internal gravity waves almost certainly play a major role in MSAO forcing, due to the absence of other strong sources, the potential for wave filtering at lower levels, and the poor model results at those heights. Finally, the modeling studies by Miyahara (1978a,b) suggested that tidal motions may be important in forcing the mean westward motions at upper levels, while that by Hamilton and Mahlman (1988) failed to achieve a westward mean in a model that excluded tidal motions. There is at present, however, virtually no observational evidence of such motions or their influences at these heights with which to compare current theoretical and modeling results.

The increasing awareness of the importance of wave forcing and a deficiency of relevant measurements of wave motions in the equatorial mesosphere provided the motivations for our use of the Jicamarca MST radar for equatorial wave and mean structure observations during 1987. This effort required a rephasing of the radar and its application to measurements of wave motions using a configuration that had not been tested previously. The location of the radar is also sufficiently far south of the equator to prevent measurements of wave and mean motions at the maximum of the QBO, SSAO, and MSAO responses. Thus, we viewed our initial use as a test of the feasibility of the approach. However, our results, reported here and in a companion paper by Hitchman et al. (1992), suggest that the experiment was a success and that additional observations may provide further insights for our understanding of equatorial dynamics.

Our results are divided in two parts. This paper focuses on gravity-wave and tidal motions, their variability and influences on the mean state, and daily variations of the mean flow in the mesosphere. The paper by Hitchman et al. (1992) presents the mean motions and momentum fluxes inferred with the Jicamarca MST radar in the stratosphere and mesosphere during our two experiments and a comparison of these results with other observations during the same periods. We begin by describing the radar configuration and the data collection, analysis, and testing procedures in section 2. Our results suggest that the data quality is high and that mean velocities and momentum fluxes should be reasonably accurate. Measured radial velocities, hourly mean winds, and momentum fluxes, along with their interpretation, are presented in section 3. These quantities reveal an energetic motion field exhibiting strong forcing of the mean flow and a high degree of variability. Discussed in section 4 are the daily mean winds and momentum fluxes. Like the hourly profiles, these display significant variability, large and persistent meridional wind shears, and a tendency for large mean winds and momentum fluxes to be negatively correlated. Also discussed in this section is evidence of inertial instability. Tidal wind fields for one of our observation periods are examined in section 5. Our conclusions are presented in section 6.

2. Experimental design and data analysis

a. Radar configuration

Our experiment used the Jicamarca MST radar near Lima, Peru (12°S, 77°W), for two ~10-day measurement campaigns during June and August 1987. The radar facility was originally designed for ionospheric research and has, in its normal configuration, a series of beam positions symmetric with respect to the local terrain (~1.4°SW of true vertical) and magnetic north (6°E of geographic north). It has, nevertheless, been used for some of the pioneering studies of atmospheric motions using the MST radar technique (Woodman and Guillen 1974; Rastogi and Woodman 1974; Rastogi and Bowhill 1976; Harper and Woodman 1977; Fukao et al. 1978, 1979, 1980).

The Jicamarca antenna consists of two superposed orthogonal linear arrays with dimensions of 300 × 300 m, each with 64 independent square modules. For our purposes, however, it was necessary to rephase the arrays to establish beam positions symmetric with respect to true vertical. This was dictated by our desire to achieve symmetric, off-vertical beam positions in order to measure momentum fluxes by the motion field in two orthogonal directions using only four simultaneous beams (Vincent and Reid 1983; Reid 1987). For this purpose, the antenna was divided into four indepen-

dent arrays, two (each 150 × 300 m) in each polarization with the long side aligned in the plane of steering. A further constraint was the ability to rephase only the 32 segments composing each array, resulting in grating lobes for large zenith angles. A zenith angle of 2.5° was selected as the best compromise between the larger values used at other facilities and the need to suppress the grating lobes sufficiently. With a half-power beamwidth of ~0.7° in the plane of steering, this was thought to be adequate to insure small beam-pointing errors in the presence of vertical aspect sensitivity. The results presented here and by Hitchman et al. (1992) seem to confirm the validity of this choice.

b. Data collection

Our experiment at the Jicamarca MST radar was performed during two periods, 15–26 June and 4–13 August 1987. The radar operated at a frequency of 50 MHz and with a peak power of ~1 MW, a pulse length of 26.67 μs, an interpulse period of 1 ms, and an 8-bit complementary pulse code, yielding a range resolution of 500 m and an average power of ~27 KW.

Radial velocities were obtained in each of four beams, all at a zenith angle of 2.5°, and at azimuths of 6°, 96°, 186°, and 276° from geographic north for daylight hours (~0600–1800 local time) during our observation periods. Velocities were obtained at 64 heights in each of two altitude intervals beginning at 19.75 km in the stratosphere and at 64.75 km in the mesosphere. Backscatter power in the stratosphere was due to neutral density fluctuations at the Bragg scale ($\lambda/2$ = 3 m at 50 MHz), while mesospheric echoes were dependent on fluctuations in the electron density at this same scale. Only daytime measurements were made because the electron density in the mesosphere (and the radar echo strength) is due primarily to photodissociation.

c. Data analysis

Velocities were estimated from 16-point power spectra composed of 16 pulse pairs that were coherently and incoherently integrated for different intervals in the stratosphere and mesosphere. Because of the smaller expected radial velocities in the stratosphere, 240 successive measurements were coherently averaged at these heights, resulting in a maximum velocity of the Doppler spectrum of 6.25 m s^{-1}. In the mesosphere, where velocities are typically larger, 64 and 80 measurements were coherently averaged for the June and August campaigns, yielding maximum Doppler velocities of 23.44 and 18.75 m s^{-1}, respectively. Incoherent averages of 5 spectra in the stratosphere and 25 (20) spectra for June (August) in the mesosphere were then performed to further decrease statistical uncertainties and reduce the data spacing and density. These choices led to velocity estimates for all four beams at 77-s and 102-s intervals for the mesospheric and stratospheric data, respectively.

Background noise for the resulting spectra was estimated as the average of the power of the three weakest spectra in each range of heights during each integration period. The signal-to-noise ratio (S/N) was then estimated from the total power at each height and velocity estimates were obtained from the first moment of the spectrum after subtracting the average noise level if S/N exceeded −6 dB. Poor velocity estimates were further screened by rejecting all radial velocities with magnitudes greater than 7.5 m s^{-1}. This threshold is smaller than the maximum velocities at these heights observed at other locations (Fritts and Yuan 1989a; Fritts et al. 1990), but served to eliminate spurious values and provide more consistent mean velocity and momentum flux estimates. Measurements were made in the stratosphere and mesosphere for 5 and 55 min during each hour.

Hourly and daily mean velocities and momentum fluxes were estimated for each interval for which at least half of the data points survived the S/N and maximum velocity thresholds described above. Mean horizontal velocities in radar coordinates (6° clockwise from geographic) were obtained by combining the mean radial velocities in opposite directions and assuming the mean vertical velocities to cancel,

$$\bar{u}(z) = \frac{U_E(R) - U_W(R)}{2\sin\theta} \tag{1}$$

and

$$\bar{v}(z) = \frac{U_N(R) - U_S(R)}{2\sin\theta}, \tag{2}$$

where $U_i(R)$ are the radial velocities in the N, S, E, and W radar directions and θ is the common zenith angle. Momentum fluxes for each time interval were computed using the method of Vincent and Reid (1983) from radial velocities following a linear trend removal,

$$\overline{u'w'}(z) = \frac{\overline{U_E^2}(R) - \overline{U_W^2}(R)}{2\sin 2\theta} \tag{3}$$

and

$$\overline{v'w'}(z) = \frac{\overline{U_N^2}(R) - \overline{U_S^2}(R)}{2\sin 2\theta}. \tag{4}$$

Analysis of the potential error in momentum flux estimates suggests a possible uncertainty with our velocity estimates and beam angles (assuming accurate beam directions) of ~1 m^2 s^{-2} for hourly values (Yamamoto et al. 1988). Inferred values larger than this should then be regarded as reliable estimates of the momentum flux for intervals longer than 1 h. The resulting data provided the basis for the analyses presented in sections 3 and 4 of this paper. For the tidal analysis discussed

in section 5, however, the computed horizontal wind fields were rotated to geographic coordinates.

d. Beam-angle testing

Because of the very small zenith angle used for our observations and the sensitivity of momentum flux estimates to beam-pointing errors, we performed a test of the symmetry of the two pairs of coplanar beams. This was done by computing the vertical velocity separately for each beam pair by adding the coplanar radial velocities and comparing the results. A lack of symmetry in the zenith angles of two coplanar beams, due either to beam-phasing errors or to an asymmetric aspect sensitivity, would manifest itself as a contamination of the computed vertical velocity by the projected horizontal velocity in that plane. Applying this test to hourly and daily mean velocities on each day of the June and August campaigns revealed no systematic differences and suggested that our pointing angles were essentially symmetric, despite the small zenith angle and the off-vertical normal orientation of the antenna field.

3. Radial velocities and hourly mean data

We present in this section examples of the radial velocity data and the hourly profiles of east and north (in radar coordinates) winds and momentum fluxes to illustrate the nature of the motions at high frequencies and their variability. Time–height cross sections of the radial velocities observed in the east beam for days 5, 6, and 10 of the August campaign (8, 9, and 13 August) are shown in Figs. 1–3, with the spacing between adjacent range gates equivalent to a radial velocity of 7.5 m s^{-1}. Corresponding hourly velocity profiles for these three days and for one day of the June campaign (19 June) are shown in Figs. 4–7. Successive eastward and northward velocity profiles, shown with solid and dashed lines, are displaced by 50 m s^{-1}.

a. Radial/vertical velocities

Clearly, the motion field in the mesosphere during our campaigns was highly active. Apparent in the radial velocities is considerable activity at frequencies near and above the local buoyancy frequency, $N \sim 0.015$ rad s^{-1} ($T \sim 7$ min). Because of our very small zenith

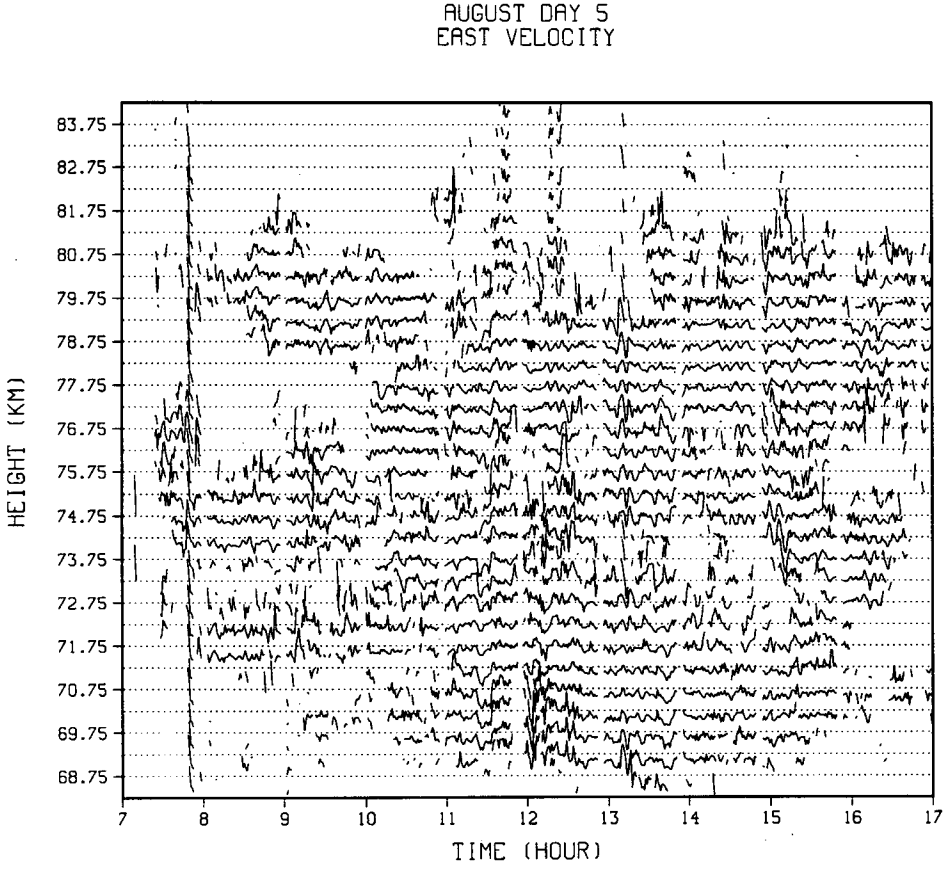

FIG. 1. Radial velocity in the east beam (zenith 2.5°, azimuth 96°) at ~1-min and 0.5-km intervals during day 5 of the August campaign (8 August).

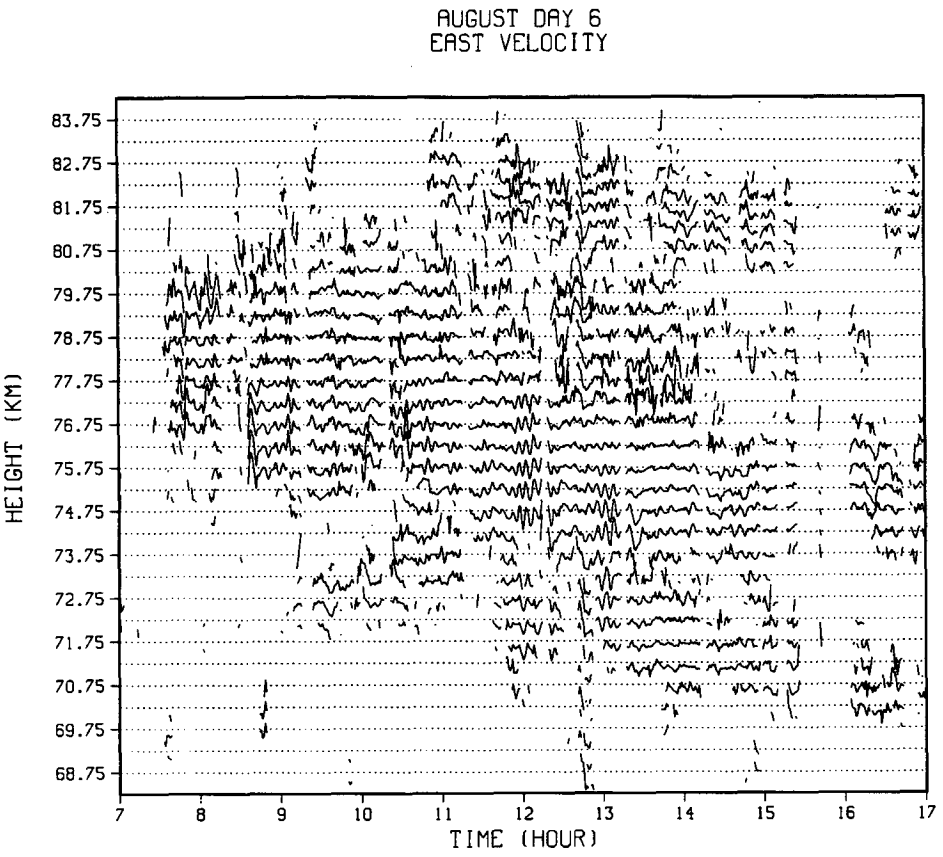

FIG. 2. As in Fig. 1 but for day 6 (9 August). Note the high frequencies and strong vertical coherence occurring at various times.

angle, the radial velocities reflect almost the total vertical velocity and only a small component of the horizontal velocity in each beam, $U_E = u \sin\theta + w \cos\theta$, for example. Thus, the high-frequency motions seen in Figs. 1–3 are primarily vertical motions and are likely to be strongly influenced by ducting and Doppler-shifting processes in a variable background flow. Motions at frequencies $\omega > N$ (seen throughout, but most prevalently in the center of Fig. 2), in particular, are indicative of wave motions being advected in their direction of propagation by a strong mean flow, yielding an apparent frequency $\omega = \omega' + k\bar{u} = k(c' + \bar{u}) = kc$ with c' and $\bar{u}$ of the same sign and $c/c' > 1$ (Fritts and VanZandt 1987).

Such motions are expected preferentially near levels at which the relative horizontal motion is a maximum in the direction of wave propagation (Chimonas and Hines 1986; Fritts and Yuan 1989b). Indeed, the vertically coherent motions with periods of ~5 min present in Fig. 2 exhibit a descent from ~76 to 73 km during the interval between ~10 and 13 local time, consistent with the downward motion of the strong maximum northward velocity seen in Fig. 5 during this same period. This suggests wave motions ducted at a relative velocity maximum and propagating toward the north, with $\omega \sim 2\omega'$ and phase speeds relative to the ground of $c \sim 2\bar{u}$. Likewise, the large-amplitude, vertically coherent motions seen in Fig. 3 near the beginning of the observation period (this wave amplitude exceeds $U_E \sim 10$ m s^{-1}) and from ~10 to 13 local time also appear to coincide with strong relative maxima of the local mean wind toward the northeast (see Fig. 6). These motions occur at smaller apparent frequencies, ω, however, suggesting either a ducted motion with $\omega \sim \omega'$ and $c \gg \bar{u}$ or a vertically propagating motion with $\omega' < N$ and large velocities and momentum flux.

b. *Horizontal velocities*

Because the radial velocities are dominated by the vertical motion field, horizontal velocities are revealed more reliably by the hourly averaged profiles for which the vertical component has been largely removed. These profiles also retain a majority of the horizontal velocity variance because most of this occurs at low (intrinsic and observed) frequencies (ω' and ω). The horizontal velocities in Figs. 4–7 exhibit a high degree

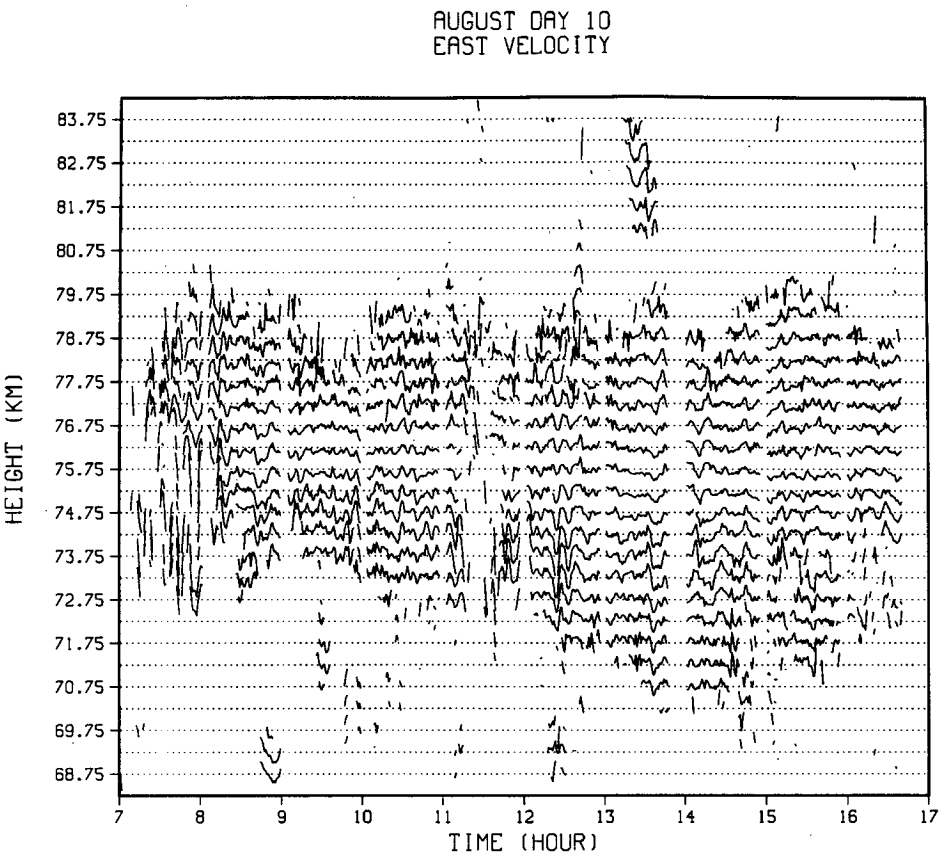

FIG. 3. As in Fig. 1 but for day 10 (13 August). Very large amplitudes at early times exceed the velocity threshold for data retention and analysis.

of variability, with characteristic vertical scales in these data of ~2–10 km. On some occasions, a downward phase progression is seen at larger vertical scales, with peak-to-peak amplitudes of ~50–100 m s^{-1} (see Figs. 5 and 6). A striking feature at other times, despite variability at smaller scales, is persistent and nearly stationary large-scale structures with $\lambda_z \sim 6$–10 km, with maximum amplitudes in the meridional plane and hourly averaged shears as large as ~0.03–0.06 s^{-1} extending over several kilometers (see Figs. 4 and 7).

Downward phase progressions are expected for vertically propagating gravity waves and tidal motions with $c/c' > 0$. Stationary phase, on the other hand, suggests either gravity-wave motions with $c \sim 0$ ($c' \sim -\bar{u}$) or other motions for which a phase progression is not anticipated. The lack of vertical phase progression and the dominance of horizontal velocity variance and wind shears by meridional motions are consistent with suggestions by Dunkerton (1981, 1983) and observations by Hitchman et al. (1987) of meridional motions at comparable vertical scales due to inertial instability of the equatorial middle atmosphere in the winter hemisphere. In fact, these observations may be the first ground-based confirmation of the presence of such motions and identification of their vertical scale and persistence. The large hourly mean shears previously noted also suggest a mesosphere that is highly unstable to dynamical instabilities with persistent mean values of the Richardson number of Ri ~ 0.25 or less. This implies as well a rich source of additional gravity wave motions and momentum transports due to instability processes within the large-scale flow. Additional discussion of low-frequency horizontal motions will be presented in sections 4 and 5, where we examine the daily averaged and tidal wind fields.

At smaller vertical scales, there is evidence of strong variability and vertical phase progressions, primarily downward (see Figs. 4–6). These motions suggest gravity waves with smaller intrinsic phase speeds ($c' \sim N/m = N\lambda_z/2\pi$) and sufficiently high frequencies to be influenced and/or filtered by the larger-scale, low-frequency structures with large amplitudes. For example, a gravity wave with a vertical wavelength $\lambda_z \sim 3$ km has an intrinsic phase speed $c' \sim 7$ m s^{-1} and should thus be highly modulated in an environment with mean wind variations ~ 10 times larger.

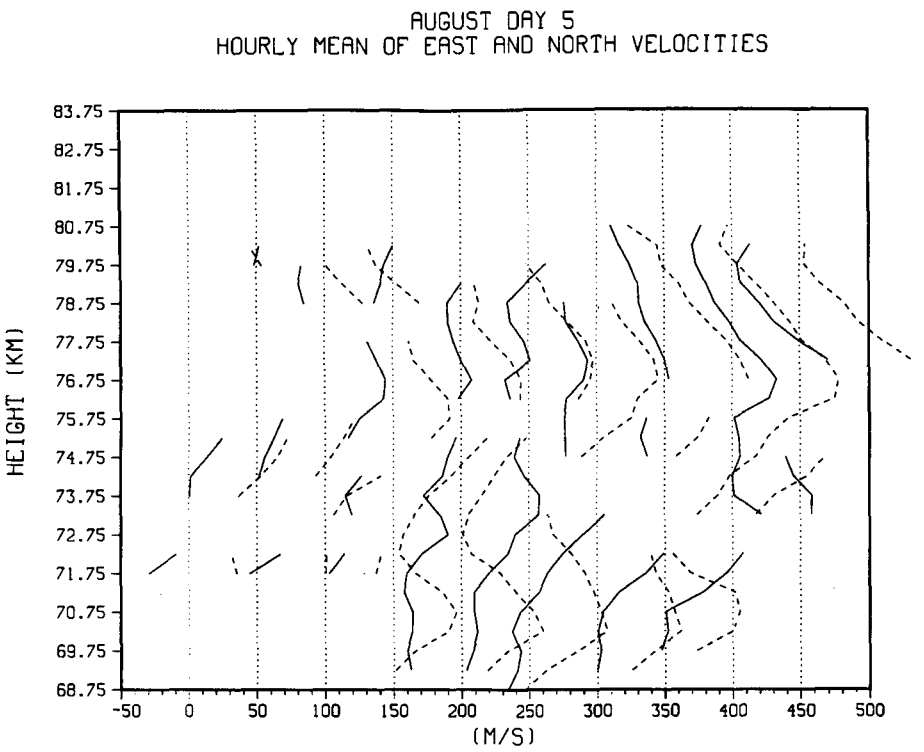

FIG. 4. Hourly mean east and north velocities (in radar coordinates) for day 5 (8 August). Note persistent structures and large vertical shears.

c. Momentum fluxes

Hourly averaged profiles of the momentum flux per unit mass, $\overline{u'w'}$ and $\overline{v'w'}$, for days 6 and 10 of the August observation and day 5 of the June campaign are presented in Figs. 8–10. These correspond to the hourly averaged wind profiles presented in Figs. 5–7. As in the previous figures, solid and dashed lines denote the zonal and meridional components (in radar coordinates).

The momentum flux profiles shown in Figs. 8–10 exhibit substantial variability in time and height, particularly in the presence of large shears in the zonal and meridional wind components. Nevertheless, they also display a high degree of consistency between adjacent profiles, which suggests, because they are independent estimates of the flux, that hourly momentum fluxes provide a valid picture of the wave field character at high observed frequencies. Three observations warrant discussion.

On two occasions, day 6 of the August campaign and day 5 of the June campaign, zonal and/or meridional momentum fluxes experienced a significant increase with height beginning at heights ~1 km below their respective maximum negative velocities (see sites labeled "a" in Figs. 5 and 8 and "b" in Figs. 7 and 10). This increase is particularly dramatic in the second, third, and fourth profiles of $\overline{v'w'}$ above ~78 km in Fig. 8 (the first hourly mean wind and momentum flux profiles were not presented for lack of sufficient data). In each of these profiles, $\overline{v'w'}$ increased from near zero to a maximum of ~60 $m^2 s^{-2}$, with increases beginning immediately below heights at which hourly averaged meridional velocities were large and negative (and ~80–100 m s^{-1} less than heights ~5 km lower). A very similar event was observed in both components at lower levels on day 5 of the June campaign (profiles 3–6 of Figs. 7 and 10). As in the event just described, zonal and meridional momentum fluxes in this case increased from values near zero at heights of ~72 km to ~30 $m^2 s^{-2}$ only ~2 km higher, slightly below maximum negative winds in the case of the meridional component and at heights of large and negative but increasing winds in the zonal component.

The events described above are remarkably like the study of gravity wave filtering and momentum flux modulation by Fritts and Vincent (1987) at Adelaide and observations of mean and variable momentum fluxes near the high-latitude summer mesopause. Fritts and Vincent (1987), extending a study by Walterscheid (1981), proposed that gravity-wave momentum fluxes would be strongly modulated due to filtering of the high-frequency wave spectrum by low-frequency tidal and gravity-wave motions, with the maximum positive

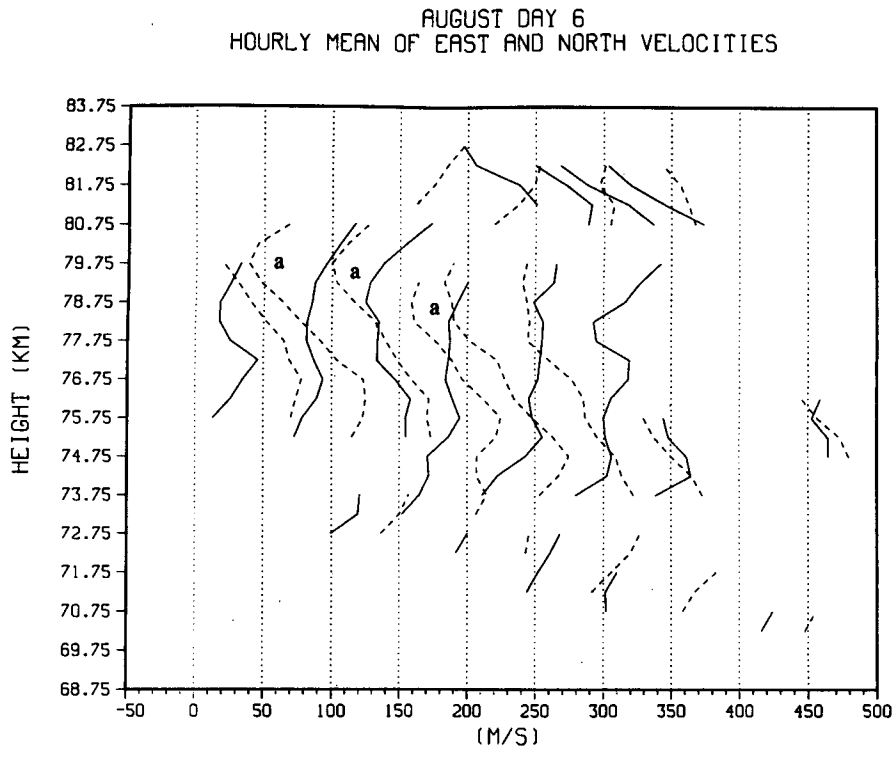

FIG. 5. As in Fig. 4 but for day 6 (9 August). Both large and small scales exhibit a strong downward phase progression.

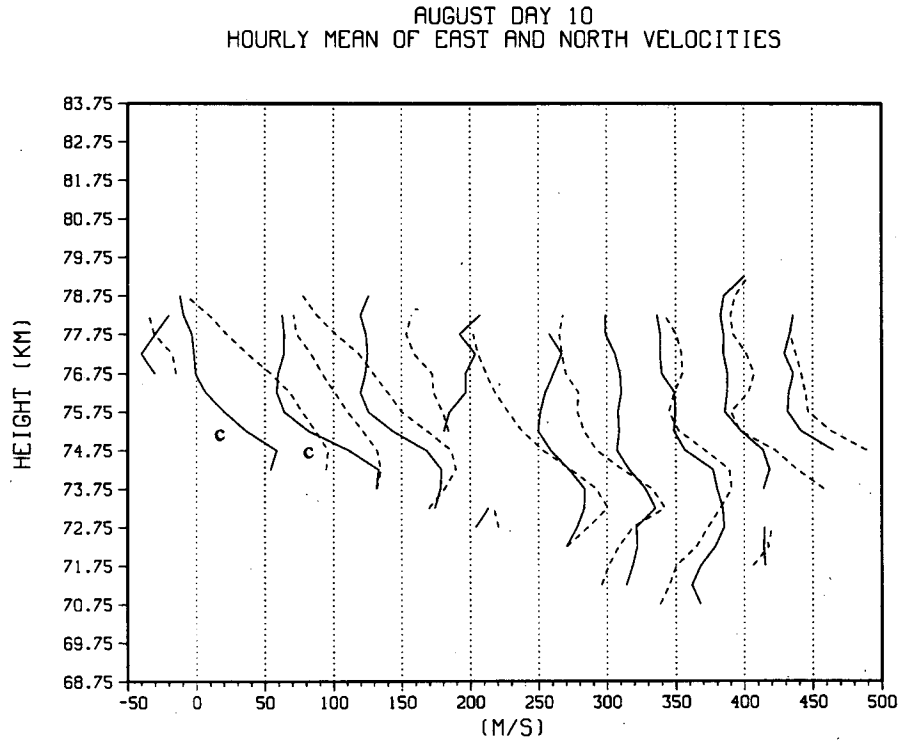

FIG. 6. As in Fig. 4 but for day 10 (13 August). Large shears and strong phase progressions occur throughout the day.

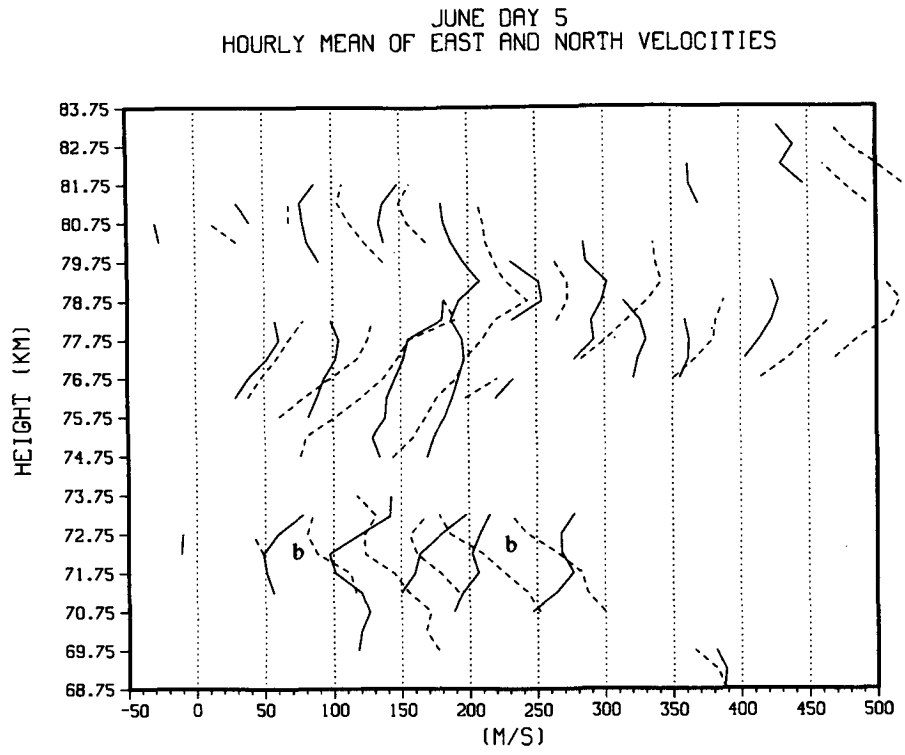

FIG. 7. As in Fig. 4 but for day 5 of the June campaign (19 June). Vertical shears and structure on this day are strong and persistent.

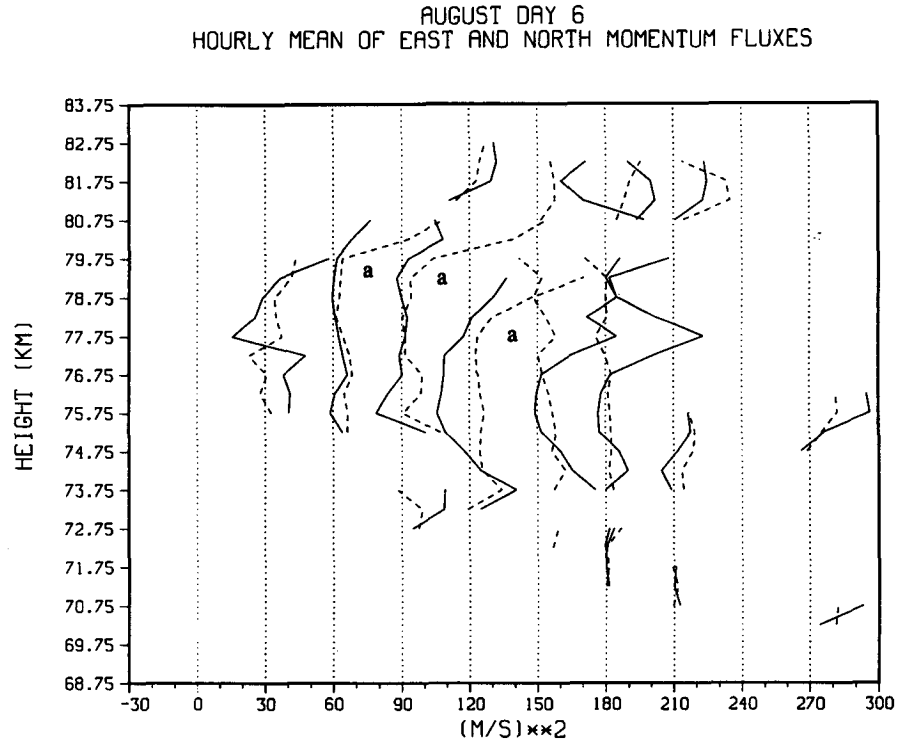

FIG. 8. Hourly mean east and north momentum fluxes (in radar coordinates) for day 6 (9 August). The large increases occurring at upper heights coincide with large negative meridional winds.

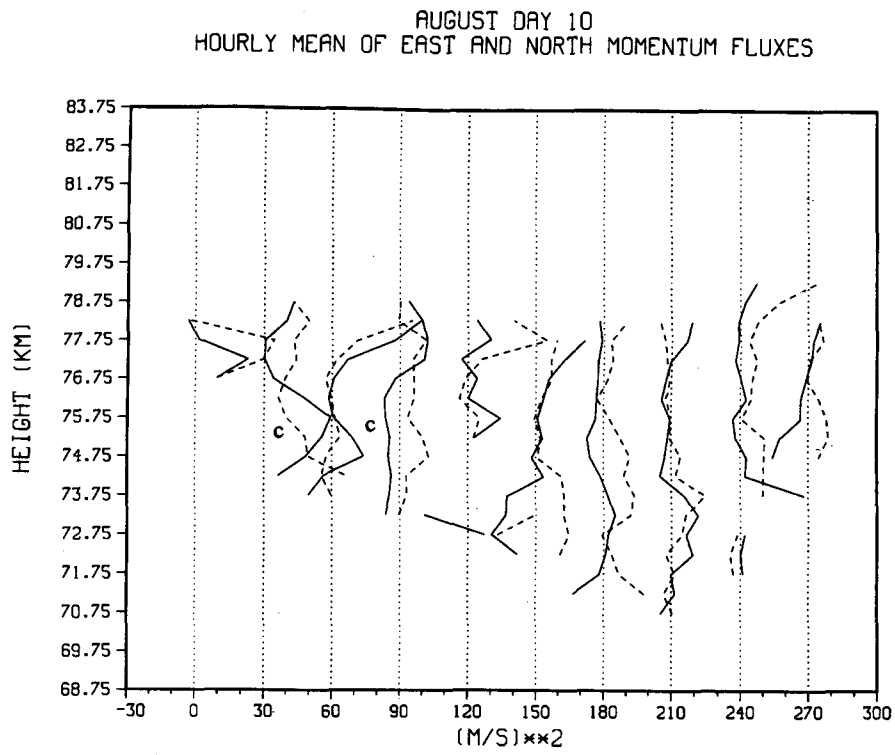

FIG. 9. As in Fig. 8 but for day 10 (13 August). Large fluxes at early times occur in regions of very large vertical shear.

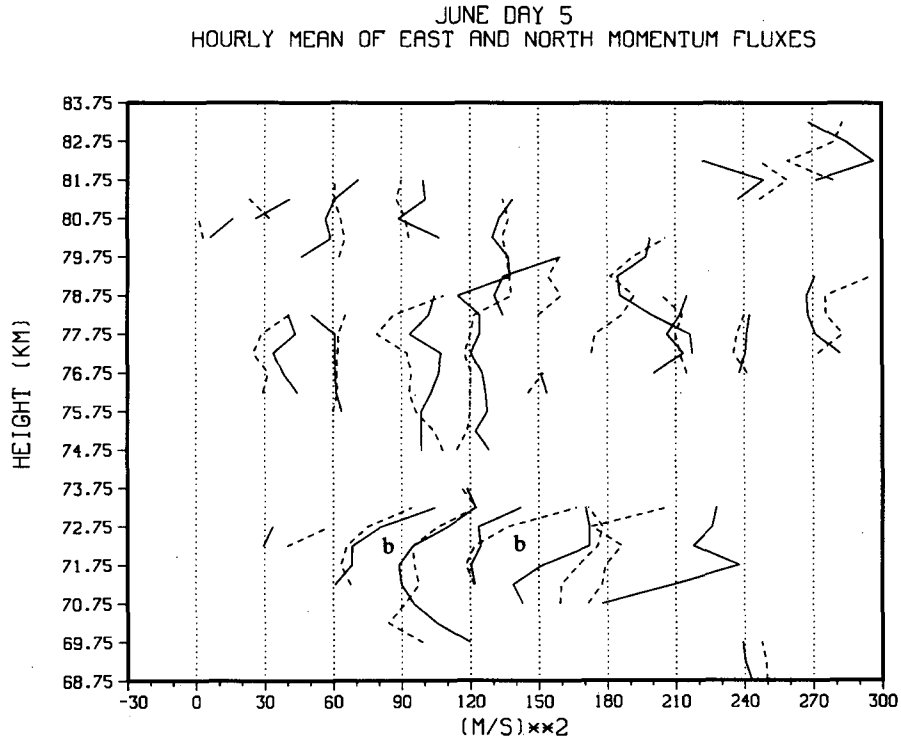

FIG. 10. As in Fig. 8 but for day 5 of the June campaign (19 June). Here, as in Fig. 8, large flux increases accompany large negative mean winds at lower levels.

(negative) fluxes occurring near or above heights of maximum negative (positive) local mean winds. This conceptual model was based on the assumption that gravity-wave amplitudes would be limited by saturation processes to values comparable with their intrinsic phase speeds, $u' \sim c - \bar{u}$, and implies that waves will achieve their maximum amplitudes and momentum fluxes near heights with c and $\bar{u}$ oppositely directed. Similar conclusions are implied by the observations of positive zonal momentum fluxes in westward mean flows, a lessening or reversal of the zonal momentum flux near the level of zonal wind reversal, and recent observations of a negative correlation of tidal wind and momentum flux components near the summer mesopause (Reid et al. 1988; Fritts and Yuan 1989a; Wang and Fritts 1990; Ruster and Reid 1990; Tsuda et al. 1990; Wang and Fritts 1991). Thus, our observations of high-frequency gravity-wave momentum flux modulation and variability at Jicamarca are consistent with similar processes occurring elsewhere and suggest a substantial role for gravity wave forcing in the equatorial middle atmosphere as well.

Another observation that we will discuss here is illustrated with the hourly mean winds and momentum fluxes in Figs. 6 and 9. This is seen in the second and third zonal-wind and momentum flux profiles near 75 km (see sites labeled "c" in Figs. 6 and 9), where there is a zonal wind shear of ~ 0.05 s^{-1} that descends slowly with time. Including the weaker shear in the meridional component, the local Richardson number is Ri ~ 0.06, assuming $N \sim 0.015$ rad s^{-1}. This implies vigorous dynamical instability and the likelihood of local momentum fluxes acting to reduce the background wind shear. The zonal momentum flux profiles support this scenario, with maximum positive values centered in the region of maximum shear in both cases. This event is distinct from those discussed earlier in that the large momentum fluxes seen in Figs. 8 and 10 appeared to arise in response to the strong southward and/or westward shears with increasing height and were maintained at large positive values above the heights of maximum negative mean winds and in the presence of positive wind shears. The occurrence of positive momentum fluxes in a positive wind shear, in particular, is impossible to explain by invoking dynamical instability and can only be associated with vertically propagating motions.

Other features of the momentum flux profiles presented in Figs. 8–10 are either less dramatic and unambiguous or show that momentum fluxes are generally smaller in the absence of strong shears or opposing mean flows. Good examples are the final five profiles on day 10 of the August campaign (Fig. 9) above ~ 74 km, where fluxes are near zero and the hourly wind profiles exhibit almost no shear (Fig. 6). Like the results of Fritts and Yuan (1989a), this suggests 1) that gravity-wave amplitudes are small due to small intrinsic phase speeds or 2) that the gravity-wave spectrum is fairly isotropic, with approximately equal components propagating in all directions, in the absence of amplitude modulation by strong local mean winds.

Together, the mean wind and momentum flux profiles previously discussed display a striking consistency with other observations and provide evidence that our Jicamarca measurements may be viewed as a reliable characterization of gravity wave influences in the equatorial regions.

4. Daily mean velocities and momentum fluxes

Presented in this section are mean winds and momentum fluxes computed daily over the full observation period (~ 10–12 h) for all 10 days of the August campaign and for 6 days of the June campaign for which adequate data were available. As before, these are presented in radar coordinates in order to avoid uncertainties associated with conversion of assumed horizontal velocities and fluxes to geographic coordinates. Note also that these mean winds are daytime averages, and may thus be influenced by diurnal tidal motions that are not properly resolved. August and June profiles are presented in Figs. 11 and 12, with winds and momentum fluxes staggered by 50 m s^{-1} and 30 m^2 s^{-2} and solid (dashed) lines representing zonal (meridional) values.

a. Wind-profile structure

The mean wind profiles (Figs. 11a and 12a) exhibit many of the same features noted in the hourly profiles presented in the previous section, particularly for those days when flow features appeared to be nearly stationary. These include very large meridional shears and dominant vertical scales of ~ 6–10 km. Large meridional shears also were seen on days during both June and August for which hourly profiles were not discussed, suggesting that such shears are present a significant fraction of the time. Maximum meridional shears in the daily profiles were ~ 0.03 s^{-1} over several kilometers for both campaigns, implying a mean state that was highly unstable, with a mean Richardson number Ri ~ 0.25, and suggesting a major role for instabilities in limiting shears and transporting horizontal momentum vertically. Successive daily mean meridional motions showed very little consistency during August, with maximum values of $\sim \pm 50$ m s^{-1} and shears shifting or reversing in an apparently random fashion. During June, however, there was some consistency in the meridional structure at upper levels, with a generally positive shear of 0.02–0.03 s^{-1} occurring at ~ 76–79 km. Zonal-mean winds generally exhibited smaller maximum amplitudes and considerably less shear, with the exception of winds at lower levels on days 5 and 6 of the August campaign. These variable

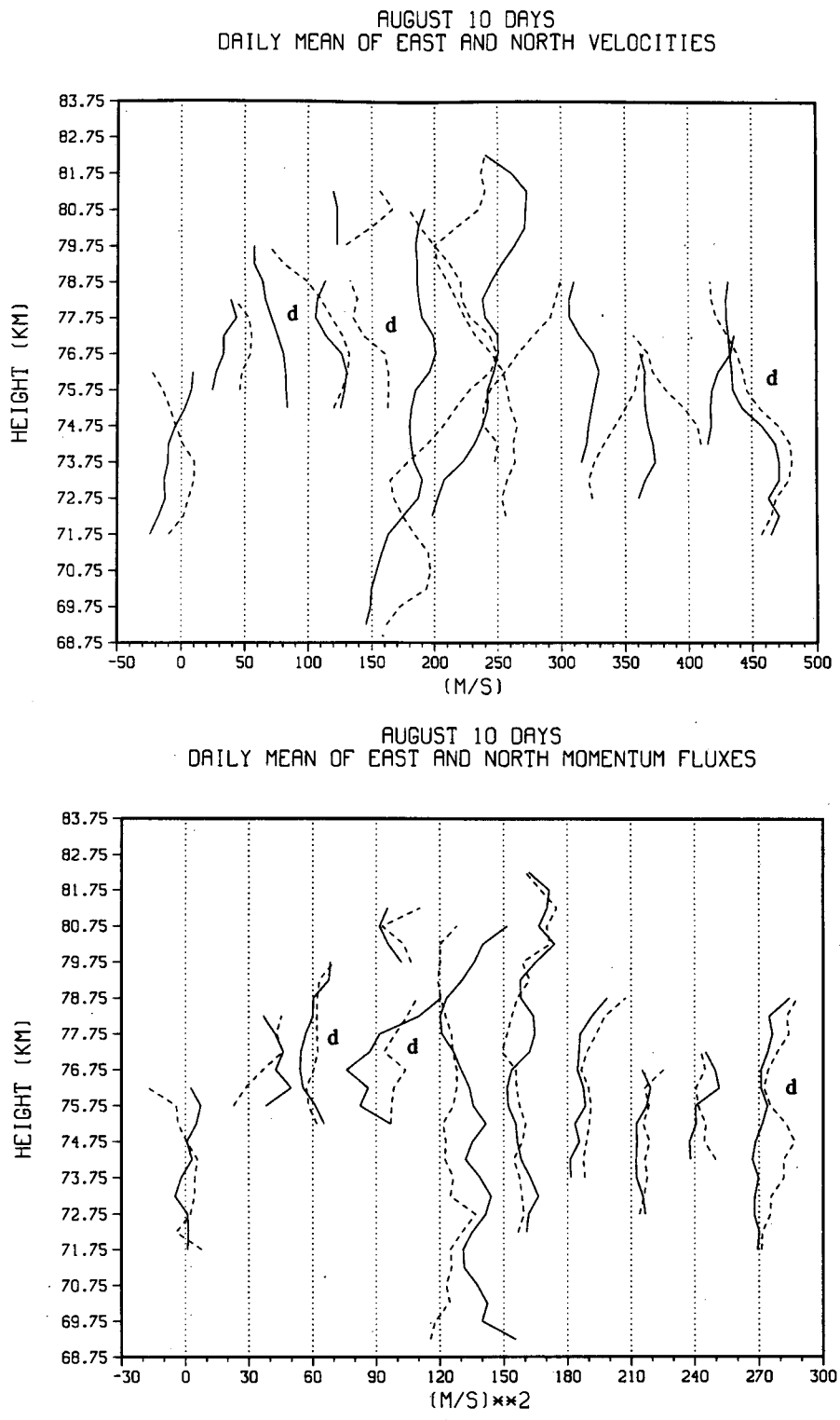

FIG. 11. Daily mean east (solid) and north (dashed) (a) velocities and (b) momentum fluxes for the 10-day August campaign. Note flow variability and large mean momentum fluxes.

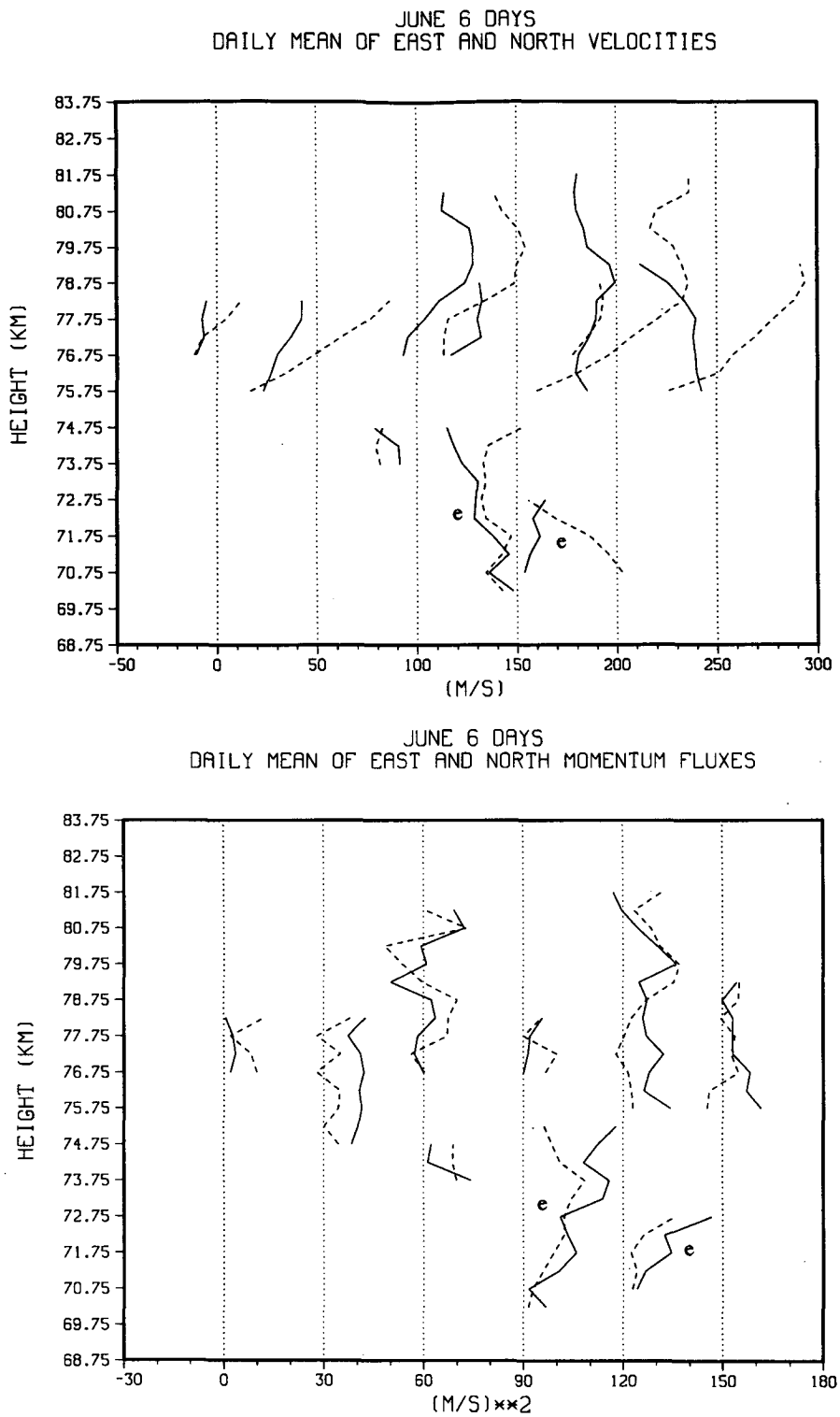

FIG. 12. As in Fig. 11 but for six days of the June campaign. The large-scale meridional velocity exhibits considerable persistence and large shears. Momentum fluxes tend to be negatively correlated with mean winds.

daily mean winds likely reflect low-frequency variability of the gravity-wave field and temporal or spatial variability of inertial instability processes.

b. *Wind and momentum flux correlations*

Daily mean momentum flux profiles reveal typical magnitudes of ~ 10 m^2 s^{-2} and maxima of ~ 30 m^2 s^{-2}. Profiles exhibit consistent variations with height, with smaller fluctuations during August and larger fluctuations during June, due to the greater fraction of data satisfying the S/N and maximum radial velocity thresholds during the August campaign. Most significant, however, is a tendency for both the mean values of wind and momentum flux and the trends in the vertical profiles to be oppositely correlated. This is not true for all cases, of course, but there are a number of clear examples that suggest this tendency in a majority of the profiles.

Perhaps the best examples of this negative correlation are in the August daily means for days 3, 4, 5, and 10 (sites labeled "d" in Fig. 11) and for days 4 and 5 in the June data at lower levels (sites labeled "e" in Fig. 12). Days 3, 4, and 10 of the August campaign show mean winds decreasing with height and momentum fluxes increasing in the opposite sense. Similarly, the zonal-mean wind profile on day 5 exhibits a clear increase with height while the zonal momentum flux decays nearly uniformly. The June profiles for days 4 and 5 likewise reveal clear negative correlations of both the mean and the trend with height, except where the zonal-mean wind is large and negative and thus favors a positive and increasing momentum flux. Other profiles suggest negative correlations as well, but are either less consistent or very limited in extent.

c. *Evidence of inertial instability*

While a primary focus of our equatorial observations was to look for gravity-wave influences on the MSAO, we also hoped to find evidence of the low-frequency Kelvin waves, tidal motions, and inertial instabilities suggested by some to be important at these heights. These topics led us to choose two campaigns spaced by ~ 6 weeks to try to capture the MSAO at a maximum (westward) amplitude and a maximum shear at times when the Kelvin wave forcing was expected to be strong. In this respect, our results were very surprising because the motion field was so variable that no evidence of Kelvin waves was found. Tidal motions were observed and are discussed in the following section.

There are several possible explanations for the lack of Kelvin wave signatures in our datasets. First, our observations took place at 12°S, well away from latitudes at which maximum Kelvin wave amplitudes are expected. Second, our observations occurred during the Southern Hemisphere winter and thus coincided with the weaker westward phase of the MSAO. This may have contributed to smaller Kelvin wave amplitudes than expected during the larger westward phase during January and February. Perhaps most significant in masking any low-frequency wave activity, however, was the enormous daily variability in the observed mean wind profiles. This variability was seen to be most apparent in the meridional wind field, where shears were enormous and characteristic vertical scales were ~ 6–10 km.

The presence and persistence of large meridional shears, possibly limited by dynamical instability processes and vertical momentum transports, provide strong evidence for an inertial instability of the form proposed by Dunkerton (1981) and suggested in the LIMS temperature analysis by Hitchman et al. (1987). Inviscid inertial instability is anticipated when $\bar{u}_y/f > (1 - \mathrm{Ri}^{-1})$ (Hitchman and Leovy 1986) in a latitude band bounded by the equator and the latitude at which $\bar{u}_y = f$ (Dunkerton 1981). These conditions occur primarily in the winter hemisphere within $\sim 25°$ of the equator (Hitchman and Leovy 1986). Inviscid theory also suggests a maximum growth rate at infinite vertical wavenumber (Dunkerton 1981). Inclusion of diffusion and zonal structure, on the other hand, yields maximum growth rates at finite vertical and zonal scales (Dunkerton 1981, 1983; Boyd and Christidis 1982). In the presence of diffusion, the maximum growth rate is expected at a vertical wavenumber

$$m_c = (N\beta/4\nu^2)^{1/5} \tag{5}$$

with a threshold shear for instability given by

$$(\bar{u}_y)_c = 2\sqrt{5}\nu^{1/5}(N\beta/4)^{2/5}, \tag{6}$$

where N is the buoyancy frequency, $\beta = df/dy$, and ν is the diffusion coefficient (Dunkerton 1981).

LIMS temperature data in the lower mesosphere suggest characteristic vertical scales of ~ 14 km and most of the temperature variance at zonal wavenumbers 1 and 2 (Hitchman et al. 1987). However, LIMS data do not extend as high as our observations and may be biased toward larger vertical scales by resolution limitations. Additionally, smaller values of diffusivity, $\nu \sim 10$ m^2 s^{-1}, that are more consistent with constraints imposed by constituent distributions in the middle atmosphere (Strobel 1989) simultaneously permit an instability threshold at smaller meridional shears, smaller vertical scales of instability, and a larger cutoff zonal wavenumber. With $N = 0.015$ rad s^{-1}, $\beta = 2.3 \times 10^{-11}$ m^{-1} s^{-1}, and $\nu = 10$ m^2 s^{-1}, we obtain a representative vertical scale of $\lambda_z \sim 7$ km, which agrees well with our observations of persistent vertical structures in the meridional wind component. If our mean wind profiles are evidence of inertial instability, then we also infer a latitudinal extent exceeding 12° and a greater persistence of such motions during June than during August, based on the continuity of successive daily profiles. The former has implications for the likely extent of inertial instability in the winter

Southern Hemisphere, while the latter may suggest instability growth and relaxation rates, intermittency of the instability, or variable zonal structure due to Rossby wave influences (Hitchman et al. 1987). Little more can be deduced, however, without a more extensive dataset.

Also expected in association with inertial instabilities is a covariance of horizontal velocities, $\overline{u'v'}$, that results in the equatorward transport of eastward momentum so as to stabilize the inertially unstable shear zone. In the Southern Hemisphere winter, this implies a positive correlation of u' and v'. Evidence for such a correlation is present in a number of the daily mean wind profiles, most notably during June, for which there is also the best evidence of persistent motions with large meridional shears and a zonal-mean wind of $\bar{u} \sim -20$ m s^{-1} (Hitchman et al. 1991).

5. Tidal wind observations

Hourly mean wind estimates obtained during August were used to examine the tidal wind structure at mesospheric heights. These data were averaged over the 10-day campaign by height and time of day to obtain profiles of mean zonal and meridional winds (in radar coordinates) for 10 h during daytime from 73.75 to 79.75 km. The resulting horizontal winds were then transformed to geographic coordinates and fitted with a mean plus tidal (12 h or 24 h) motion using a least-squares procedure. June data were not used for this analysis because there was not a sufficient number of hourly values, due to imposed radial velocity and S/N thresholds, to compose representative averages over the campaign. Fits to the diurnally varying zonal and meridional winds for the 12-h period are shown in Fig. 13, while the mean and tidal amplitudes and hours of maximum are shown for each component in Fig. 14.

Before discussing these results, it must be noted that there is, in principle, significant ambiguity in the periodicity of the diurnal winds needed to account for the observed profiles. This arises because wind data were not obtained during nighttime and hourly wind averages are subject to some uncertainty (Crary and Forbes 1983). As a result, fits to the August mean data were obtained with nearly equal statistical confidence for both diurnal and semidiurnal fits. This precluded a simultaneous fit to both tidal components. Despite this, we were able to discriminate between the two tidal motions on the basis of the computed tidal amplitudes and the implied zonal and meridional mean winds.

Diurnal and semidiurnal fits were obtained over the same height range and data interval. The diurnal fits, however, led to inferred amplitudes ranging from ~20 to 100 m s^{-1}, a mean zonal wind of $\bar{u} \sim -90$ m s^{-1} at upper heights, a mean meridional wind of $\bar{v} \sim 50$–80 m s^{-1} at all heights, and an almost constant phase with height. But these inferred amplitudes are inconsistent with other observations and tidal theory (Groves 1980; Forbes 1982a,b; Vial 1986), the phase estimates are not consistent with that expected for the diurnal tide, and the inferred mean motions are impossible to reconcile with our current understanding of the mean structure of this region. These results led us to conclude that diurnal tidal motions, if present during our campaign, must have contributed only a small fraction to the observed diurnal variability. Nevertheless, our results do not preclude the presence of diurnal tidal amplitudes of ~10–20 m s^{-1} and correspondingly smaller variations in the implied mean motions.

Semidiurnal fits to the hourly mean wind data (Fig. 13), in contrast to the diurnal results, appear to be in qualitative agreement with observed and theoretical tidal amplitudes and phases extrapolated from other heights and latitudes. The amplitudes and times of maximum amplitude (Fig. 14a and 14b) show a tendency for amplitude growth with height, with $u' \sim 5$–20 m s^{-1} and $v' \sim 10$–30 m s^{-1}, a maximum zonal component leading the maximum meridional motion by ~2–4 h, and some variation of phase with height. Inferred amplitudes are somewhat larger than those anticipated by Forbes (1982b) at upper levels, perhaps suggesting that part of the daily variability was associated with the diurnal tidal motion. The phase lag between the zonal and meridional components is consistent with that expected for the semidiurnal motion, but the phase variability suggests a possible interference of the various motions contributing to the diurnal wind field. Thus, because of the uncertainties associated with inferring tidal motions from ten hourly wind profiles, these results should be viewed as only qualitative estimates of the semidiurnal tidal motions at this location. The mean wind profiles obtained after removal of semidiurnal wind components are shown in Fig. 14c and reveal a mean motion field with weak cross-equatorial flow and a zonal-mean wind near zero at lower levels and exhibiting a weak westward shear at greater heights. Additional discussion of the mean wind profiles in the stratosphere and mesosphere during our observational campaigns is presented by Hitchman et al. (1992).

6. Summary and conclusions

We have presented an analysis of the motion field in the mesosphere at periods less than one day observed with the Jicamarca MST radar near Lima, Peru, in two ~10-day campaigns during June and August 1987. Mean motions and momentum fluxes computed for these periods in the stratosphere and mesosphere are presented and compared with other data by Hitchman et al. (1992). These campaigns represent the first use of the radar in a new symmetric beam configuration designed for studies of wave momentum transports and influences on the QBO, SSAO, and MSAO in the equatorial middle atmosphere.

Our observations provide evidence of a highly vari-

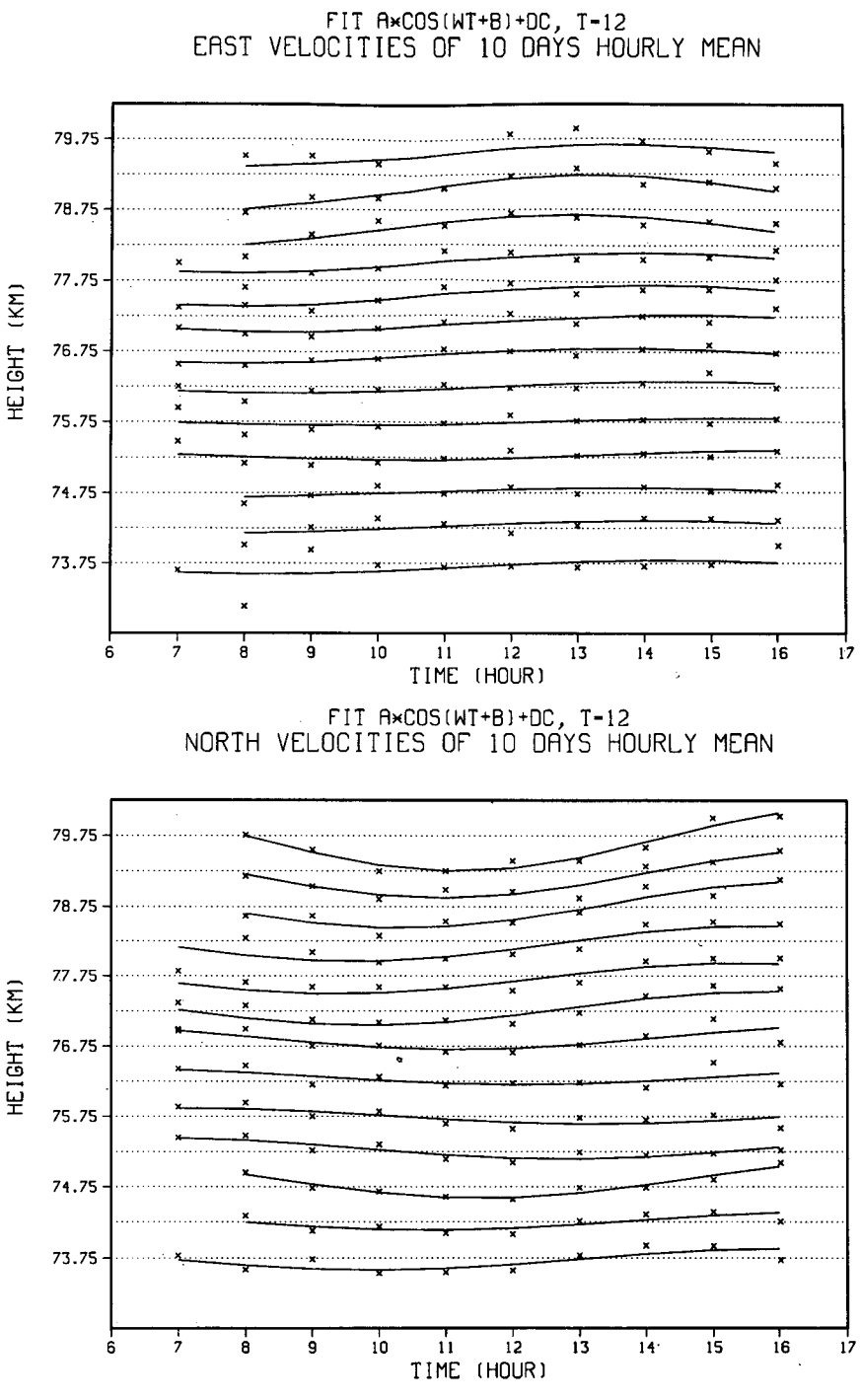

FIG. 13. Semidiurnal fits to the (a) east and (b) north hourly velocities averaged over the August campaign (in geographic coordinates).

able motion field, with periods ranging from ~5 min to many hours. Individual radial velocity estimates were found to reflect primarily vertical motions with high intrinsic frequencies, while hourly mean motions were more representative of the horizontal motion field. Hourly mean horizontal winds exhibited strong phase progressions at times, with vertical scales of ~2–10 km. On other occasions, the meridional component exhibited very large and persistent shears with characteristic vertical scales of ~6–10 km. At times these shears approached ~0.03–0.06 s^{-1}, suggesting local mean Richardson numbers of Ri ~ 0.06–0.25.

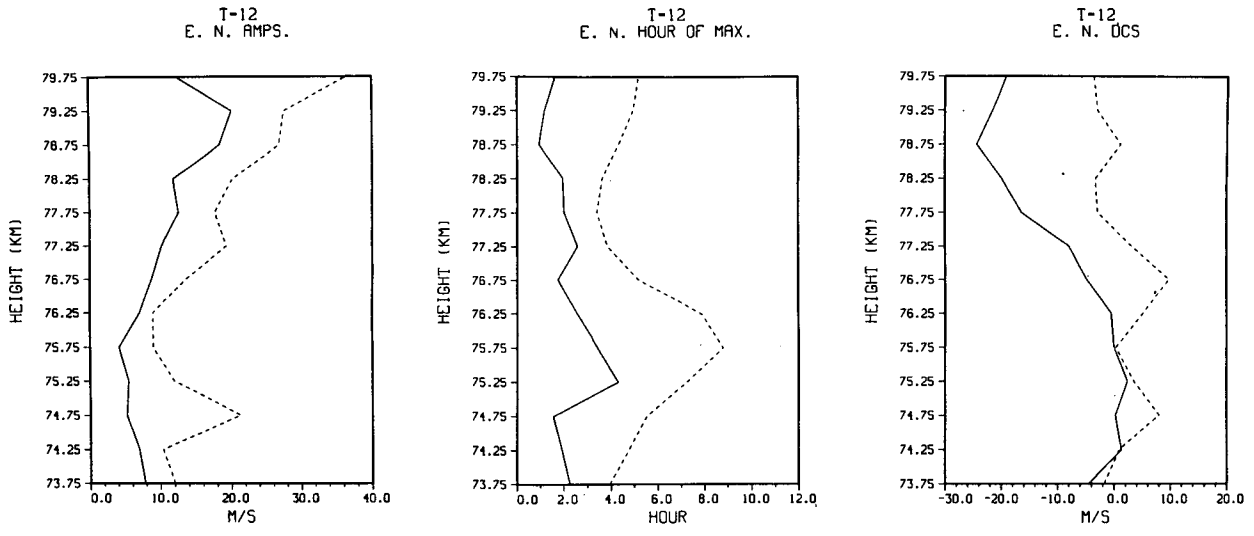

FIG. 14. (a) Semidiurnal tidal amplitudes, (b) hours of maximum, and (c) residual means inferred for the east (solid) and north (dashed) components during the August campaign.

Corresponding momentum flux profiles, reflecting fluxes due to waves with periods <1 h, were found to display a high degree of consistency between successive profiles and to suggest a modulation and filtering of the wave spectrum. This filtering was manifested as a rapid growth of the momentum flux with height beginning near or below heights at which the hourly mean wind in that direction achieved a large negative value, consistent with previous observational studies and theoretical expectations (Fritts and Vincent 1987; Fritts and Yuan 1989a). Momentum fluxes also achieved large positive values in the presence of very large positive shears, suggesting vertical momentum transports in response to shear instabilities due to the small local Richardson numbers. Momentum fluxes and variations tended to be small when mean wind was small.

Daily mean wind profiles were found to be highly variable in August and somewhat more consistent during the June campaign. Large meridional shears were observed during both periods, suggesting the presence of inertial instabilities at vertical scales of ~6–10 km. These observations were seen to be similar to other inferences of inertial instability in the equatorial middle atmosphere (Dunkerton 1981; Hitchman et al. 1987) and to imply strong meridional circulations, dynamical instabilities, and momentum transports as consequences. Daily momentum flux profiles revealed mean values of ~ 10 m^2 s^{-2} with maxima of ~ 30 m^2 s^{-2}. Also apparent in the daily mean profiles was a tendency for horizontal winds and momentum fluxes to be negatively correlated, suggesting a statistical response to filtering of the gravity-wave field by the local environment. Perhaps because of the considerable daily variability in mean wind profiles, no evidence of Kelvin wave activity was obtained.

Our observations provided evidence of a semidiurnal tidal motion with horizontal winds of ~5–10 m s^{-1} near 74 km and ~20–30 m s^{-1} near 80 km. A diurnal tidal motion was seen not to account for all of the observed diurnal variability, but may have contributed motions with amplitudes of ~10–20 m s^{-1}. Semidiurnal tidal phases were found to exhibit somewhat variable structure with height and show the zonal wind maximum to have led the meridional by ~2–4 h. The variable phases inferred for the semidiurnal component suggest a possible superposition of tidal modes.

Taken together, our results imply a dynamically very active equatorial middle atmosphere, with strong and variable gravity-wave forcing due to filtering processes and large momentum transports, tidal amplitudes growing with height, and vigorous inertial instabilities likely resulting in instability and transports on other scales. These motions exhibit a considerable potential for influencing the equatorial middle atmosphere on many scales. This, in turn, provides strong impetus for additional studies using radar techniques.

Acknowledgments. Support for this research was provided by the National Science Foundation under Grant ATM-8609507 and by the SDIO/IST and managed by the Office of Naval Research under Contract N00014-90-J-1271. The Jicamarca Radio Observatory is operated by the Instituto Geofisico del Peru with support from the National Science Foundation. The authors would also like to thank R. A. Vincent and S. Fukao for helpful comments on the manuscript.

REFERENCES

Angell, J. K., and J. Korshover, 1970: Quasi-biennial, annual and semiannual zonal wind and temperature harmonic amplitudes

and phases in the stratosphere and low mesosphere of the Northern Hemisphere. *J. Geophys. Res.*, **75**, 543–550.

Belmont, A. D., D. G. Dartt, and G. D. Nastrom, 1975: Variations of stratospheric zonal winds, 20–65 km, 1961–1971. *J. Appl. Meteor.*, **14**, 585–594.

Boyd, J. P., 1982: The influence of meridional shear on planetary waves, Part II: Critical latitudes. *J. Atmos. Sci.*, **39**, 770–790.

——, and Z. D. Christidis, 1982: Low wavenumber instability on the equatorial beta-plane. *Geophys. Res. Lett.*, **9**, 769–772.

Chimonas, G., and C. O. Hines, 1986: Doppler ducting of atmospheric gravity waves. *J. Geophys. Res.*, **91**, 1219–1230.

Crary, D. J., and J. M. Forbes, On the extraction of tidal information from measurements covering a fraction of a day. *Geophys. Res. Lett.*, **10**, 580–582.

Delisi, D. P., and T. J. Dunkerton, 1988a: Equatorial semiannual oscillation in zonally averaged temperature observed by the *Nimbus-7* SAMS and LIMS. *J. Geophys. Res.*, **93**, 3899–3904.

——, and ——, 1988b: Seasonal variation of the semiannual oscillation. *J. Atmos. Sci.*, **45**, 2772–2787.

Devarajan, M., C. A. Reddy, and C. R. Reddi, 1985: Rocket observations of Kelvin waves in the upper stratosphere over India. *J. Atmos. Sci.*, **42**, 1873–1879.

Dunkerton, T. J., 1981: On the inertial stability of the equatorial middle atmosphere. *J. Atmos. Sci.*, **38**, 2354–2364.

——, 1982: Theory of the mesopause semiannual oscillation. *J. Atmos. Sci.*, **39**, 2681–2690.

——, 1983: A nonsymmetric equatorial inertial instability. *J. Atmos. Sci.*, **40**, 807–813.

——, 1985: A two-dimensional model of the quasi-biennial oscillation. *J. Atmos. Sci.*, **42**, 1151–1160.

——, and D. P. Delisi, 1985a: Climatology of the equatorial lower stratosphere. *J. Atmos. Sci.*, **42**, 376–396.

——, and ——, 1985b: The subtropical mesospheric jet observed by the *Nimbus-7* Limb Infrared Monitor of the Stratosphere. *J. Geophys. Res.*, **90**, 10 681–10 692.

Forbes, J. M., 1982a: Atmospheric tides, 1, Model description and results for solar diurnal component. *J. Geophys. Res.*, **87**, 5222–5240.

——, 1982b: Atmospheric tides, 2, The solar and lunar semidiurnal components. *J. Geophys. Res.*, **87**, 5241–5252.

Fritts, D. C., and T. E. VanZandt, 1987: The effects of Doppler shifting on the frequency spectra of atmospheric gravity waves. *J. Geophys. Res.*, **92**, 9723–9732.

——, and R. A. Vincent, 1987: Mesospheric momentum flux studies at Adelaide, Australia: Observations and a gravity wave/tidal interaction model. *J. Atmos. Sci.*, **44**, 605–619.

——, and L. Yuan, 1989a: Measurement of momentum fluxes near the summer mesopause at Poker Flat, Alaska. *J. Atmos. Sci.*, **46**, 2569–2579.

——, and ——, 1989b: An analysis of gravity wave ducting in the atmosphere: Eckart's resonances in Thermal and Doppler ducts. *J. Geophys. Res.*, **94**, 18 455–18 466.

——, U.-P. Hoppe, and B. Inhester, 1990: A study of the vertical motion field near the high-latitude summer mesopause during MAC/SINE. *J. Atmos. Terres. Phys.*, **52**, 927–938.

Fukao, S., S. Kato, S. Yokai, R. M. Harper, R. F. Woodman, and W. E. Gordon, 1978: One full-day radar measurement of stratospheric winds over Jicamarca. *J. Atmos. Terres. Phys.*, **40**, 1331–1337.

——, T. Sato, S. Kato, R. M. Harper, R. F. Woodman, and W. E. Gordon, 1979: Mesospheric winds and waves over Jicamarca on May 23–24, 1974. *J. Geophys. Res.*, **84**, 4379–4386.

——, ——, I. Hirota, and S. Kato, 1980: A preliminary radar observation of long-period waves in the tropical mesosphere over Jicamarca. *J. Geophys. Res.*, **85**, 1955–1957.

Gao, X.-H., W.-B. Yu, and J. L. Stanford, 1987: Global features of the semiannual oscillation in stratospheric temperatures and comparisons between seasons and hemispheres. *J. Atmos. Sci.*, **44**, 1041–1048.

Gray, L. S., and J. A. Pyle, 1986: The semiannual oscillation and equatorial tracer distributions. *Quart. J. Roy. Meteor. Soc.*, **112**, 387–407.

Groves, G. V., 1980: Seasonal and diurnal variations of middle atmosphere winds. *Phil. Trans. Roy. Soc. London*, **A296**, 19–41.

Hamilton, K., 1982: Rocketsonde observations of the mesospheric semiannual oscillation at Kwajalein. *Atmos.–Ocean*, **20**, 281–286.

——, and J. D. Mahlman, 1988: General circulation model simulation of the semiannual oscillation of the tropical middle atmosphere. *J. Atmos. Sci.*, **45**, 3212–3235.

Harper, R. M., and R. F. Woodman, 1977: Preliminary multiheight radar observations of waves and winds in the mesosphere near Jicamarca. *J. Atmos. Terr. Phys.*, **39**, 959–963.

Hirota, I., 1978: Equatorial waves in the upper stratosphere and mesosphere in relation to the semiannual oscillation of the zonal wind. *J. Atmos. Sci.*, **35**, 714–722.

——, 1980: Observational evidence of the semiannual oscillation in the tropical middle atmosphere. *Pure Appl. Geophys.*, **118**, 217–238.

Hitchman, M. H., and C. B. Leovy, 1986: Evolution of the zonal mean state in the equatorial middle atmosphere during October 1978–May 1979. *J. Atmos. Sci.*, **43**, 3159–3176.

——, and ——, 1988: Estimation of the Kelvin wave contribution to the semiannual oscillation. *J. Atmos. Sci.*, **45**, 1462–1475.

——, ——, J. C. Gille, and P. L. Bailey, 1987: Quasi-stationary, zonally asymmetric circulations in the equatorial middle atmosphere. *J. Atmos. Sci.*, **44**, 2219–2236.

——, K. W. Bywaters, D. C. Fritts, L. Coy, E. Kudeki, and F. Surucu, 1992: Ten-day mean winds and momentum fluxes over Jicamarca, Peru, during June and August 1987. *J. Atmos. Sci.*, **49**, 2372–2383

Holton, J. R., and R. S. Lindzen, 1972: An updated theory for the quasi-biennial cycle of the tropical stratosphere. *J. Atmos. Sci.*, **29**, 1076–1080.

Hopkins, R., 1975: Evidence of polar–tropical coupling in stratospheric zonal wind anomalies. *J. Atmos. Sci.*, **32**, 712–719.

Miyahara, S., 1978a: Zonal mean winds induced by vertically propagating atmospheric tidal waves in the lower thermosphere, Part I. *J. Meteor. Soc. Japan*, **56**, 86–97.

——, 1978b: Zonal mean winds induced by vertically propagating atmospheric tidal waves in the lower thermosphere, Part II. *J. Meteor. Soc. Japan*, **56**, 548–558.

Nastrom, G. D., and A. D. Belmont, 1975: Periodic variations in stratospheric–mesospheric temperature from 20–65 km at 80°N to 30°S. *J. Atmos. Sci.*, **32**, 1715–1722.

Naujokat, B., 1986: An update of the observed quasi-biennial oscillation of the stratospheric winds over the tropics. *J. Atmos. Sci.*, **43**, 1873–1877.

Plumb, R. A., 1977: The interaction of two internal waves with the mean flow: Implications for the theory of the quasi-biennial oscillations. *J. Atmos. Sci.*, **34**, 1847–1858.

——, and A. D. McEwan, 1978: The instability of a forced standing wave in a viscous stratified fluid: A laboratory analog of the quasi-biennial oscillation. *J. Atmos. Sci.*, **35**, 1827–1839.

——, and R. C. Bell, 1982: A model of the quasi-biennial oscillation on an equatorial beta-plane. *Quart. J. Roy. Meteor. Soc.*, **108**, 335–352.

Rastogi, P. K., and R. F. Woodman, 1974: Mesospheric studies using the Jicamarca incoherent-scatter radar. *J. Atmos. Terr. Phys.*, **36**, 1217–1231.

——, and S. A. Bowhill, 1976: Gravity waves in the equatorial mesosphere. *J. Atmos. Terres. Phys.*, **38**, 51–60.

Reed, R. J., 1965: The quasi-biennial oscillation of the atmosphere between 30 and 50 km over Ascension Island. *J. Atmos. Sci.*, **22**, 331–333.

——, 1966: Zonal wind behavior in the equatorial stratosphere and lower mesosphere. *J. Geophys. Res.*, **71**, 4223–4233.

Reid, I. M., 1987: Some aspects of Doppler radar measurements of the mean and fluctuating components of the wind field in the upper middle atmosphere. *J. Atmos. Terr. Phys.*, **49**, 467–484.

——, R. Ruster, P. Czechowsky, and G. Schmidt, 1988: VHF radar

measurements of momentum flux in the summer polar mesosphere over Andenes (69°N, 16°E), Norway. *Geophys. Res. Lett.*, **15**, 1263–1266.

Ruster, R., and I. M. Reid, 1990: VHF radar observations of the dynamics of the summer polar mesopause region. *J. Geophys. Res.*, **95**, 10 005–10 016.

Salby, M. L., D. L. Hartmann, P. L. Bailey, and J. C. Gille, 1984: Evidence of equatorial Kelvin modes in *Nimbus-7* LIMS. *J. Atmos. Sci.*, **41**, 220–235.

Strobel, D. F., 1989: Constraints on gravity wave induced diffusion in the middle atmosphere. *Pure Appl. Geophys.*, **130**, 533–546.

Takahashi, M., 1984: A numerical model of the semi-annual oscillation. *J. Meteor. Soc. Japan*, **62**, 52–68.

Tsuda, T., Y. Murayama, M. Yamamoto, S. Kato, and S. Fukao, 1990: Seasonal variation of momentum flux in the mesosphere observed with the MU radar. *Geophys. Res. Lett.*, **17**, 725–728.

Vial, F., 1986: Numerical simulations of atmospheric tides for solstice conditions. *J. Geophys. Res.*, **91**, 8955–8969.

Vincent, R. A., and I. M. Reid, 1983: HF Doppler measurements of mesospheric momentum fluxes. *J. Atmos. Sci.*, **40**, 1321–1333.

Wallace, J. M., 1973: General circulation of the tropical lower stratosphere. *Rev. Geophys. Space Phys.*, **11**, 191–222.

——, and V. E. Kousky, 1968: Observational evidence of Kelvin waves in the tropical stratosphere. *J. Atmos. Sci.*, **25**, 900–907.

Walterscheid, R. L., 1981: Inertio-gravity wave induced accelerations of mean flow having an imposed periodic component: Implications for tidal observations in the meteor region. *J. Geophys. Res.*, **86**, 9698–9706.

Wang, D.-Y., and D. C. Fritts, 1990: Mesospheric momentum fluxes observed by the MST radar at Poker Flat, Alaska. *J. Atmos. Sci.*, **47**, 1512–1521.

——, and ——, 1991: Evidence of gravity wave-tidal interaction observed near the summer mesopause at Poker Flat, Alaska. *J. Atmos. Sci.*, **48**, 572–583.

Woodman, R. F., and A. Guillen, 1974: Radar observations of winds and turbulence in the stratosphere and mesosphere. *J. Atmos. Sci.*, **31**, 493–505.

Yamamoto, M., T. Sato, P. T. May, T. Tsuda, S. Fukao, and S. Kato, 1988: Estimation error of spectral parameters of MST radars obtained by least squares fitting method and its lower bound. *Radio Sci.*, **23**, 1013–1021.

Yanai, M., and I. Maruyama, 1966: Stratospheric wave disturbances propagating over the equatorial Pacific. *J. Meteor. Soc. Japan*, **44**, 291–294.